

FEDSM-ICNMM2010-30840

NOZZLE EFFECTS IN THERMAL WIND TUNNELS

Zhu Wang
Exa Corporation
Livonia, MI, USA
wangzhu@exa.com

Jaehoon Han
Exa Corporation
Livonia, MI, USA
jaehoon@exa.com

Ales Alajbegovic
Exa Corporation
Livonia, MI, USA
ales@exa.com

ABSTRACT

Presented is an investigation of the wind-tunnel nozzle effects on the thermal performance within passenger vehicle underhood area. The Lattice-Boltzmann Equation (LBE) based flow solver is coupled with the system tool to solve for airflow and temperature distribution around the passenger vehicle in the wind tunnel. Several simulations with different nozzle sizes were performed. The simulation results are compared with airflow, temperature, and heat exchangers heat rejection measurements in the thermal wind tunnel. Good agreement is observed confirming that nozzle geometry dominates the airflow around the vehicle. The results show that different nozzle sizes can produce flows that have almost the same macroscopic characteristics while at the same time have subtle differences that can be very important for the vehicle design.

NOMENCLATURE

LBE solver; coupled simulation; underhood flow; digital wind tunnel (DWT).

INTRODUCTION

The measurements of cooling airflows and temperatures in passenger vehicles are commonly performed in thermal wind tunnels. Thermal wind tunnels are smaller in size than the aerodynamic wind tunnels. Their purpose is to provide representative flow conditions in the underhood and underbody areas. They are also equipped to perform various temperature measurements of the heat exchanger performances and temperatures of both surfaces and air. Solar radiation effects can be included using reflectors.

The ability to simulate cooling airflow within a wind tunnel is of great importance for the design of vehicles. Srinivasan *et al.* [1] presented vehicle thermal management simulation with an omni-tree meshing technology for rapid mesh generation using Navier-Stokes flow solvers. The cooling airflow simulations using traditional computational fluid dynamics (CFD) solvers coupled with heat exchanger calculations for passenger cars were presented by [1], [2], [3], [4], and for trucks by [5], [6], [7].

Fortunato *et al.* [8] used the Lattice-Boltzmann Equation (LBE) solver for the cold flow simulation over the entire car including the underhood and a Navier-Stokes solver for the underhood flow. The velocity field on the entrance surfaces into the underhood area calculated by the LBE solver was used as the inlet boundary condition to the Navier-Stokes solver calculation. Fully coupled simulations between the LBE solver and a system simulation tool for the heat exchanger were presented by Alajbegovic *et al.* [9], [10]. A detailed validation of the cooling package using coupling with the system simulation tool was shown in [11]. The simulation capability presented here used the same experimental data for the thermal performance study.

In this study, several simulations of the cooling airflows were conducted for a passenger car. The simulations were performed in an aero-dynamic wind tunnel, which is also called digital wind tunnel (DWT). The study will focus on the investigation of nozzle effects in the wind tunnel. The airflow in the wind tunnels is provided through a large nozzle in front of the vehicle. The nozzle sizes are varied to provide larger range

of air velocities. The impact of nozzle size on the airflow distribution in front and under the vehicle has been compared to the simulation results. The purpose of the study is to provide recommendations for the thermal wind tunnel design and to identify guidance for measurements evaluation.

The rest of the paper is organized as follows. First, the mathematical model is presented, followed by the description of simulation methodology. After that, the simulation results are shown and thermal performance is compared for all simulations. At the end of the paper, the conclusions are summarized.

MATHEMATICAL MODEL

The flow simulation is performed using the Lattice-Boltzmann Equation (LBE) based solver (PowerFLOW 4.1c). The Lattice-Boltzmann solvers are numerically efficient, accurate and robust. The numerical efficiency allows handling of lattices with very large voxel counts. It is quite normal to have 100 million voxels for a full vehicle analysis. This enables to resolve as large as possible span of turbulence scales and in this way increase the accuracy of the predictions. Properties of the Boltzmann equation allow for an improved treatment of fluid interactions with the wall surface. Surface elements (or surfels), are designed as active elements that interact with the neighboring lattice elements. The combination of both large lattices and dynamic surface treatment allow accurate representation of surfaces without the need for geometry simplification.

The Boltzmann equation formulates the problem in terms of a distribution function $f(x,v,t)$, which is the number of molecules at position x with speed v . The Boltzmann equation can be written in the following form:

$$\frac{\partial f}{\partial t} + v \cdot \nabla f = C(x,v,t) \quad (1)$$

Here the left hand side represents the convective motion of particles and the right hand side is the collision term that expresses interactions between particles. PowerFLOW uses the BGK collision operator by Bhatnagar *et al.* [12]. It can be expressed as follows,

$$C(x,v,t) = -\frac{f - f_{eq}}{\tau} \quad (2)$$

where τ is the relaxation time of the fluid and f_{eq} is the equilibrium Maxwellian distribution function. The Boltzmann equation along with the BGK operator is discretized on a three dimensional cubic lattice using a D3Q19 model as shown in Figure 1. The resulting finite difference equation enables the solution of the distribution function.

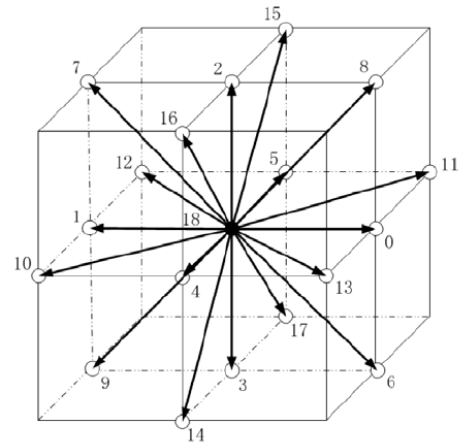


Figure 1. D3Q19 cubic lattice for Boltzmann equation

Integral moments of the distribution function along with the ideal gas law can then be used to calculate the velocities and pressures. It can be shown rigorously that the Lattice Boltzmann formulation thus outlined is equivalent to solving the time dependent compressible Navier Stokes equation. A review of the fundamentals of the lattice Boltzmann method can be referred to Chen and Doolen [13].

Earlier use of Lattice-Boltzmann equation in fluid flow simulations was done by Frisch, Hasslacher, & Pomeneau [14]. After that, significant efforts were made to develop Lattice-Boltzmann flow solver [13], [15], [16]. Small scale turbulence effects are modeled using a modified $k-\epsilon$ model based on the original RNG formulation [17], [18]. This LBE based description of turbulent fluctuation carries flow history and upstream information, and contains high order terms to account for the nonlinearity of the Reynolds stress [19]. This is contrasted with typical Navier-Stokes solvers, which tend to use the conventional linear eddy viscosity based on the Reynolds stress closure models. Turbulence and temperature equations are solved on the same lattice using a modified Lax-Wendroff-like explicit time marching finite difference scheme. Simulations presented in this work were performed using the flow solver described in the following references [20], [21], [22], [23], [24].

SIMULATION METHODOLOGY

The presented simulation methodology is based on coupled simulations between the flow and system solvers. Therefore, the following three major simulation components are:

1. Flow modeling with the Lattice-Boltzmann Equation solver
2. System tool heat exchanger model
3. Automatic coupling between the flow solver and system tool

SYSTEM SIMULATIONS

System tools are used to model and analyze multi-domain, intelligent systems and to predict their multi-disciplinary performance. The components of a system are described by analytical models representing the hydraulic, pneumatic, electric, thermal and mechanical behavior of the system components.

In this study, the heat rejection for the heat exchangers is calculated by the system tool using LMS Imagine.Lab AMESim. Figure 2 shows the system tool model of the charge air cooler, radiator and condenser respectively.

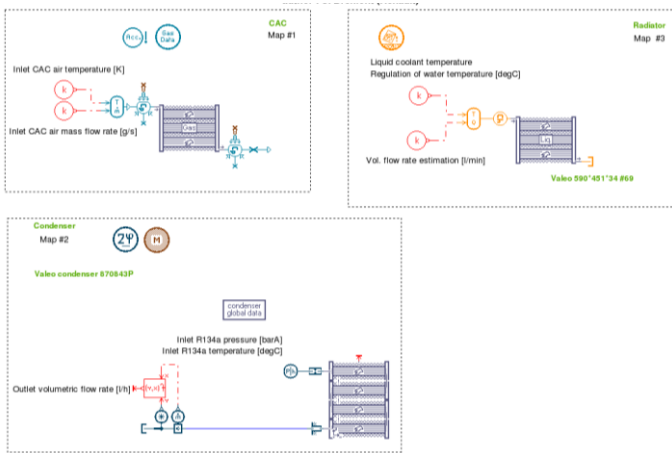


Figure 2. System tool heat exchanger model

COUPLING PROCESS

The flow solver and system tool two-way coupling is implemented via an automated process using scripts. The coupling process involves the extraction and exchange of flow data distributions on each of the heat exchanger inlet and outlet surfaces. Flow solver provides the cooling air velocity and temperature fields, and the system tool calculates the distribution of the heat source and provides the heat flux distribution back to the flow solver. The coupling process is described in Figure 3.

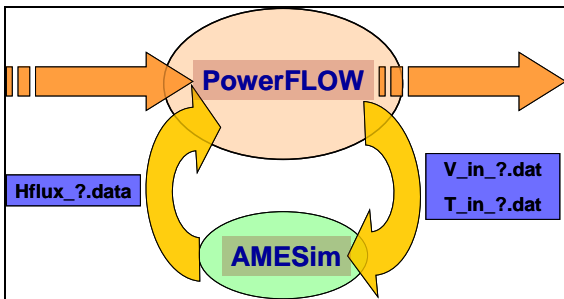


Figure 3. General two-way coupling scheme

SIMULATION DETAILS

The vehicle used in this study was Renault Scenic II. The low speed (40 km/h) and “fan on” conditions were applied. Figure 4 shows the vehicle, its underhood geometry and cooling package details. The flow solver simulates air velocity and temperature distributions in the entire domain including the engine compartment and vehicle exterior. The details of the geometry preparation, case setup and boundary conditions are similar to thermal wind tunnel simulation presented in [11].

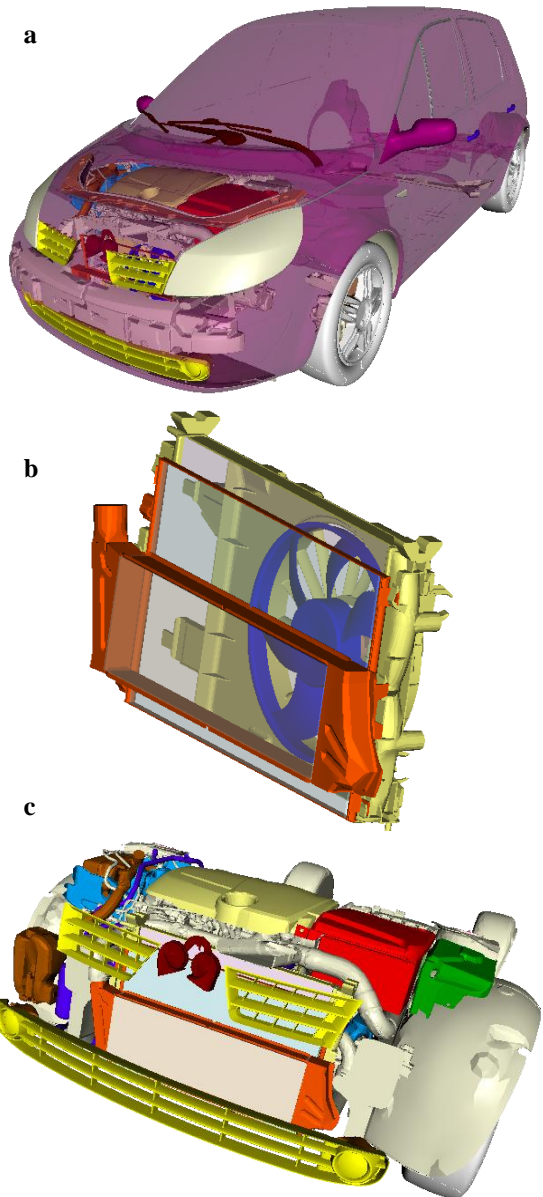


Figure 4. a.) Vehicle geometry, b.) Cooling package details and c.) Underhood geometry

Figure 5 shows the placement of the heat exchangers. The charge-air-cooler, condenser and radiator are placed slightly

tilted in the underhood area. Position of the heat exchangers has crucial impact on their thermal performance.

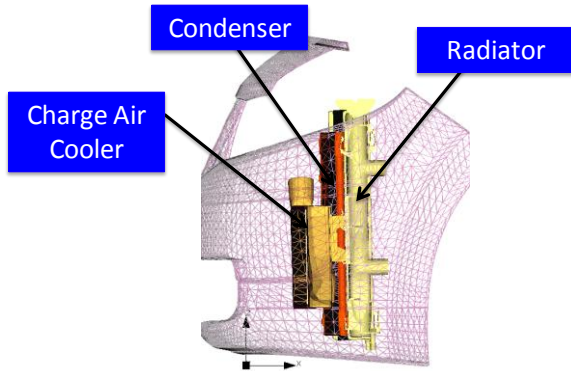


Figure 5. Locations of the heat exchangers (side view)

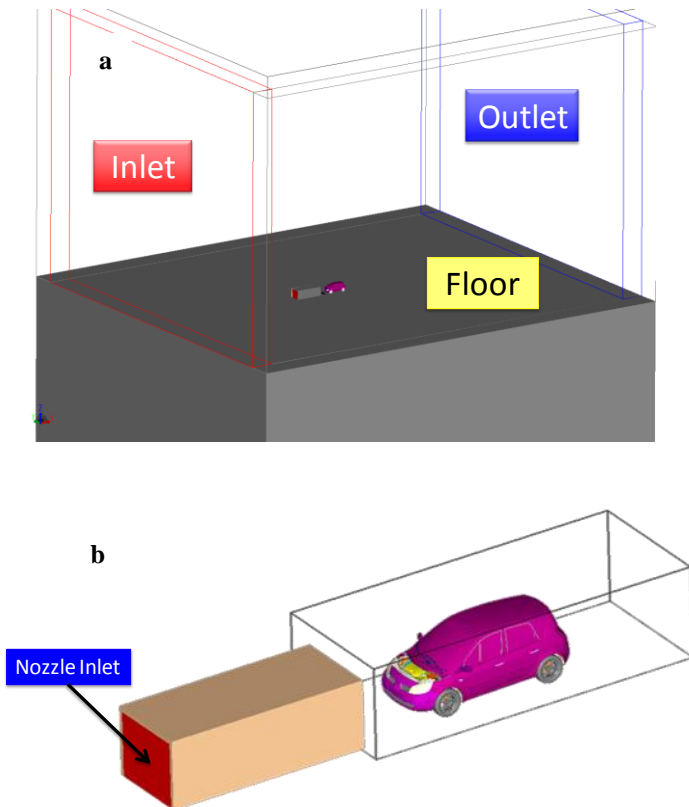


Figure 6. a.) Vehicle in Digital Wind Tunnel, b.) Nozzle in front of Vehicle

Vehicle placement in the digital wind tunnel and geometry with the nozzle profile are shown in Figure 6. Simulations were focused on evaluating the thermal performance of the underhood cooling package.

In this study, three nozzle sizes are simulated for comparison, and they are shown in Figure 7. The nozzle height

in case 1 is the same as in the thermal wind tunnel simulation [11] in order to acquire similar thermal performance. Case 2 and 3 with different nozzle sizes, 3/4 and one half nozzle height in case 1, are simulated to study the impact of the nozzle size on the underhood cooling airflow. The thermal wind tunnel is shown in Figure 8.

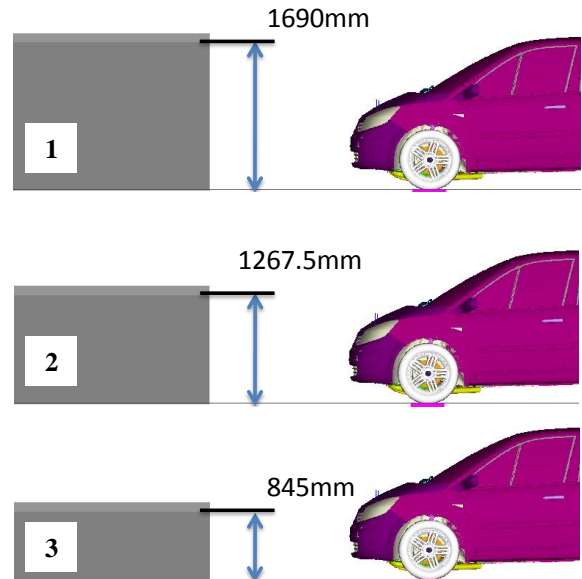


Figure 7. Three vehicle nozzle heights: 1.) 1690 mm, 2.) 1267.5 mm and 3.) 845 mm

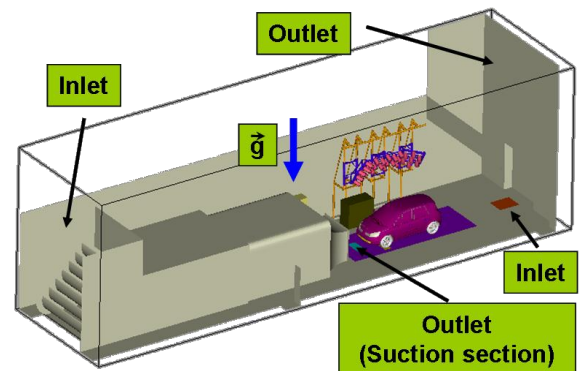


Figure 8 Thermal wind tunnel and boundary conditions

BOUNDARY CONDITIONS

Vehicle cooling package performance was measured in the thermal wind tunnel at an upstream velocity of 40 km/h. The distance between the nozzle exit and the bumper of the vehicle was 1.5 m. In order to obtain similar results as measured, the same wind speed and simulation conditions were applied to the digital wind tunnel simulations in this study. The rotation speed of the fan was 2700 rpm. Heat exchanger conditions used during the experiments are summarized in Table 1. The

numbers in *italic* were used as input conditions to the simulations.

WIND	Air Velocity	km/h	<i>39.7</i>
	Air Temperature	°C	<i>44.8</i>
FAN	Voltage	V	<i>13.0</i>
	Intensity	A	<i>32.5</i>
CHARGE AIR COOLER	Mass flow rate	kg/h	<i>165.6</i>
	Inlet temperature	°C	<i>173.2</i>
	Outlet temperature	°C	<i>64.8</i>
CONDENSER	Inlet pressure	bar	<i>25.0</i>
	Outlet pressure	bar	<i>23.6</i>
	Volumetric flow rate	l/h	<i>136.8</i>
	Inlet temperature	°C	<i>106.3</i>
	Outlet temperature	°C	<i>67.46</i>
RADIATOR	Volumetric flow rate	l/h	<i>4799</i>
	Inlet temperature	°C	<i>100.2</i>
	Outlet temperature	°C	<i>95.9</i>

Table 1. Simulation conditions

RESULTS AND DISCUSSION

In this section, the results of the three coupled simulations are presented and the impact of the nozzle size on thermal performance is discussed based on the comparison with the simulation results. First, the results using the full nozzle size (case 1) are presented to demonstrate the capability of the simulation approach. The simulation results of case 2 and 3 are compared next in studying the impact of different nozzle sizes on the cooling airflow through the cooling package.

DWT SIMULATION RESULTS (CASE 1)

Based on comparison with measurements obtained in the thermal wind tunnel [11], the results of the full nozzle size in the digital wind tunnel have shown a lower thermal performance of cooling airflow due to lower mass flow rates through heat exchangers.

The temperature fields at front and back planes of the charge-air-cooler are shown in Figure 9. Figure 10 shows temperature distribution at the back plane of the condenser. Heating can be observed as the air passes through the heat exchangers. Figure 11 shows the velocity behind the radiator. The rotating fan accelerates the flow in front of it. Figure 12 shows velocity and temperature distributions on the fan mid-plane.

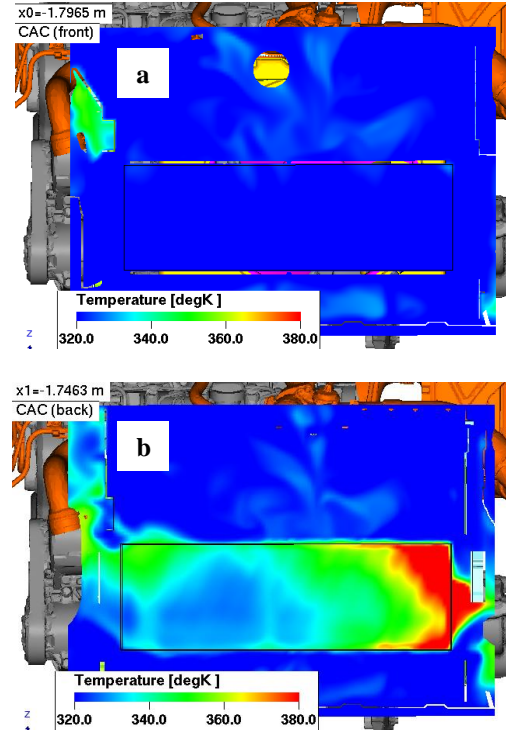


Figure 9. Temperature distribution in front and back plane of the charge-air-cooler

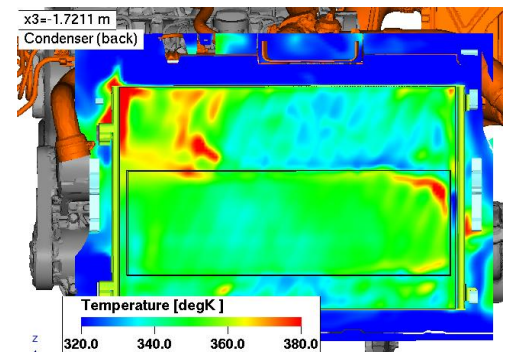


Figure 10. Temperature distribution behind the condenser

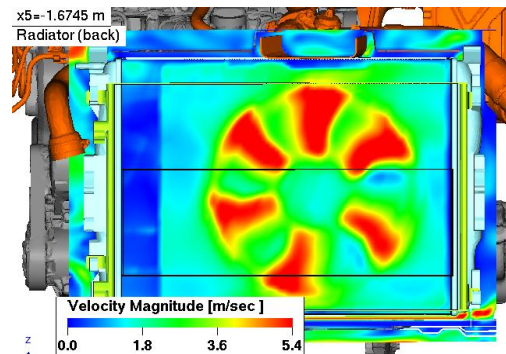


Figure 11. Velocity distribution behind the radiator

The results for cases 2 and 3 are visually very similar compared to case 1 with only small differences in temperature and velocity distributions around the cooling package. The averaged velocity, front and back temperature and heat rejections are summarized in the next sub-section for comparison.

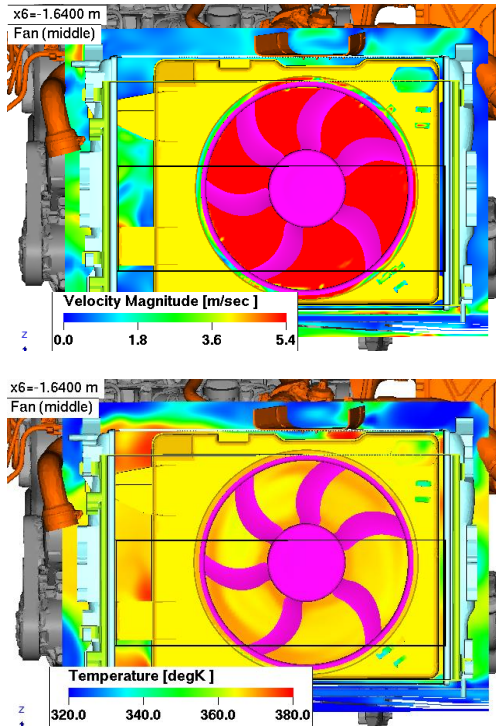


Figure 12. Velocity and temperature distribution on the fan mid-plane

The details of the predicted flow velocity field within the underhood region are shown in Figure 13. Velocity field magnitude is depicted on several critical vertical planes. These planes are top left grille, fan center, center vertical plane and top right grille. Higher velocities at grille inlets and fan area can be clearly seen. Due to the complex geometry, the flow within the underhood region is very complex as well. Recirculation, separation and local acceleration can be observed to occur almost everywhere.

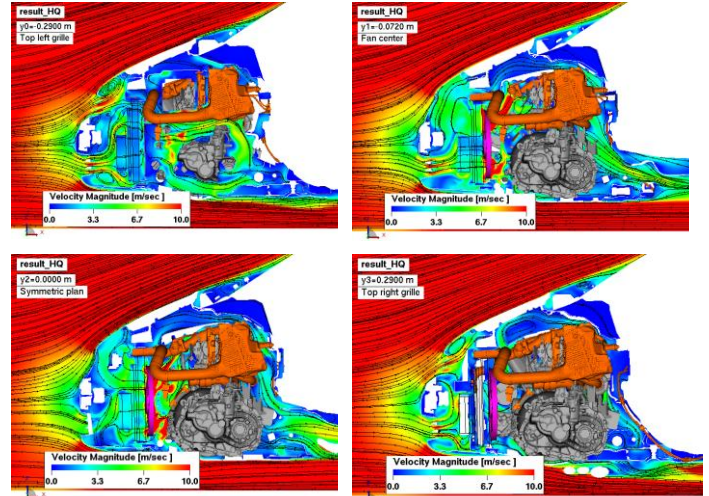


Figure 13. Velocity on y-plane in the underhood region

Streamlines and temperature field are depicted for the same vertical planes as in Figure 13. The details of the temperature field in the underhood region are shown in Figure 14. The aerodynamic and thermal behavior of the cooling airflow can be easily captured, which can be useful for the packaging optimization of the underhood components.

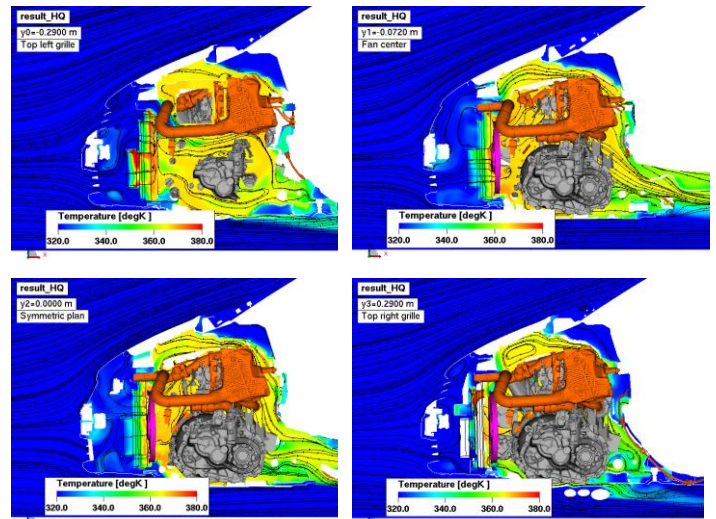


Figure 14. Temperature field on the y-plane in the underhood region

Figure 15 and Figure 16 show the velocity and temperature distributions separately on several horizontal planes. These locations are bottom grille, fan center and top grilles.

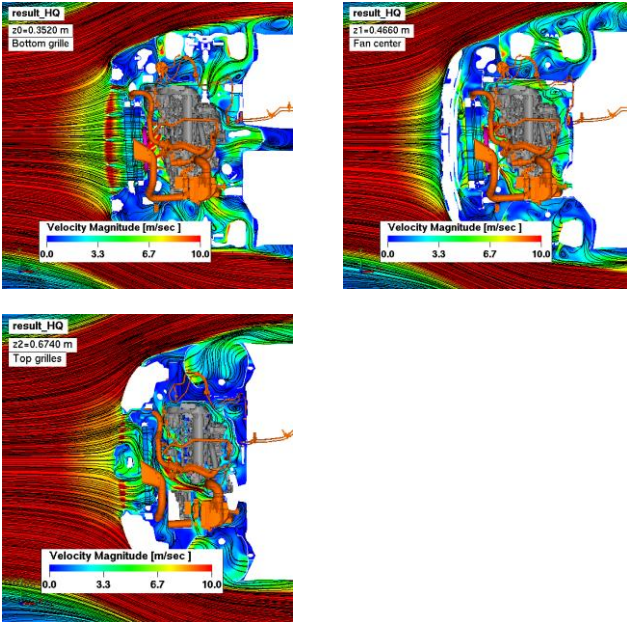


Figure 15. Velocity on the z-plane in the underhood region

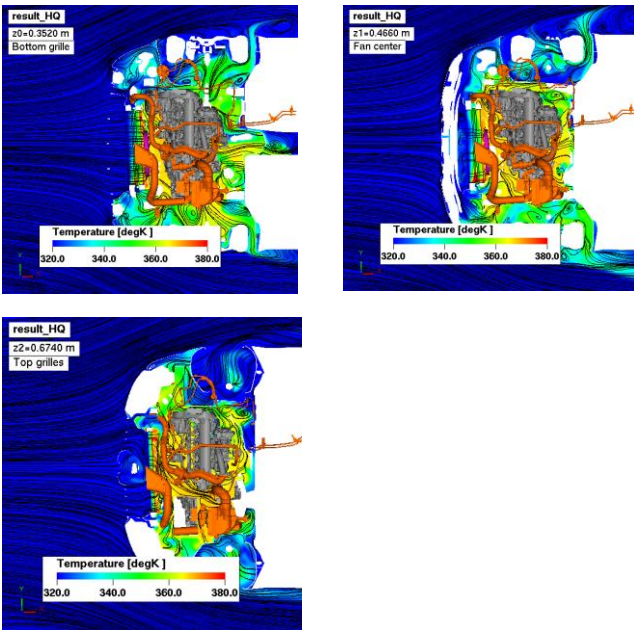


Figure 16. Temperature on the z-plane in the underhood region

The obtained results demonstrate the overall capability of the presented simulation approach to predict both flow field parameters and the performance of the cooling package.

THERMAL PERFORMANCE COMPARISON

Simulation results for case 1 have shown capability of solving air flow, including flow structure, temperature distribution, and thermal performance of the cooling package.

In this sub-section, the differences of the air flow and thermal performance due to different nozzle sizes are studied. The temperature, velocity and heat rejection are compared for the three cases.

The velocity fields at the center plane of the vehicle are shown in Figure 17. It can be seen that nozzle height directly influences the thickness of the air flow in front of the vehicle. Thickness of the high speed zone around the vehicle reduces with nozzle size. The most pronounced wake structure change can be observed in case 3.

The air flow direction after reaching the bumper changes most in the half nozzle case and obvious flow separation was identified after the windshield. Less air mass flow rate is expected for the top grilles in case 3.

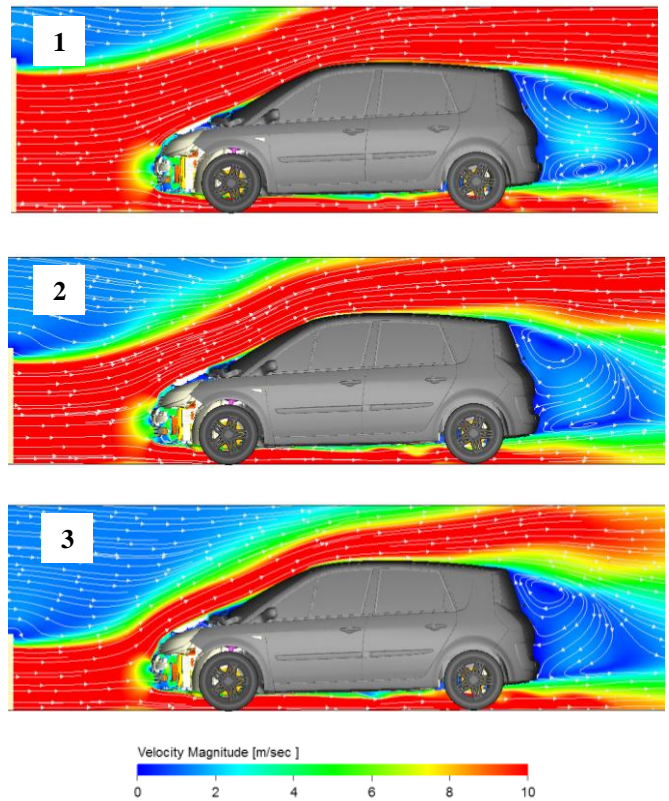


Figure 17. Velocity at Center Plane: a.) Full nozzle size, b.) Three quarter of full size, and c.) Half full nozzle size

Figure 18, Figure 19, and Figure 20 show streamlines colored by the velocity magnitude within the underhood area. Due to the different nozzle heights, more air flow passes through the top grille in case 1. In case 3, the top grille is more restrictive and less air flows through it.

The air flow structure in front of the condenser is similar for all three cases. The cooling airflow in front of the condenser is highly non-uniform. The two airflow streams coming through

the top and bottom grilles mix with each other. More recirculation of the cooling airflow can be observed right on the top and bottom sides of the condenser for case 3. Due to the fan nozzle no obvious air recirculation downstream of the fan can be observed.

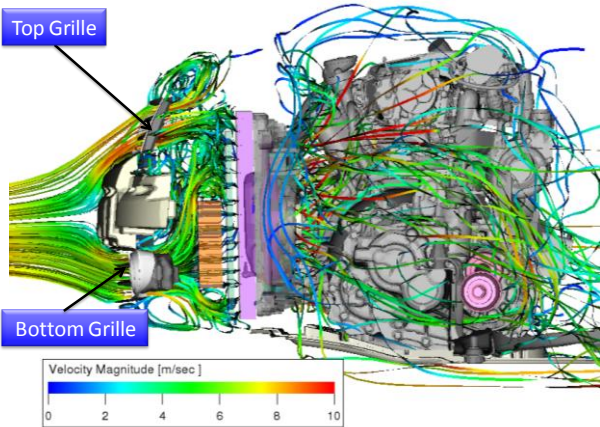


Figure 18. Streamlines around the heat exchangers (Case 1)

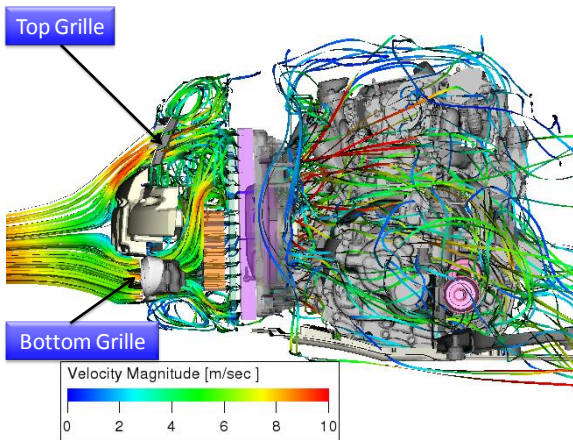


Figure 19. Streamlines around the heat exchangers (Case 2)

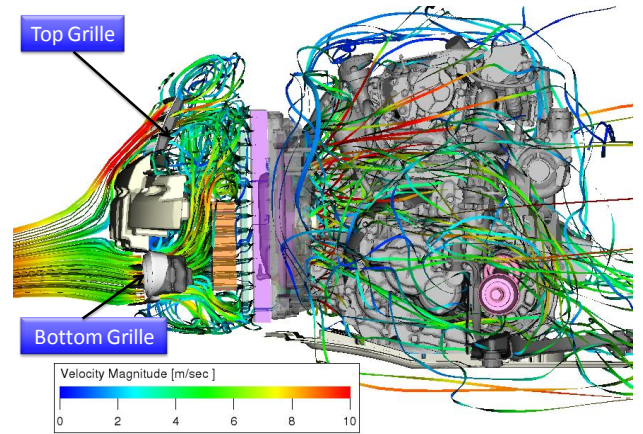


Figure 20. Streamlines around the heat exchangers (Case 3)

Figure 21 and Figure 22 compare velocity distributions and streamlines at fan center plane between cases 1 and 3. Larger velocity magnitude found in front of the top condenser and at back side of the engine in case 1 due to more air flow through the top grille. Higher heat rejection is expected for condenser in case 1 than in case 3.

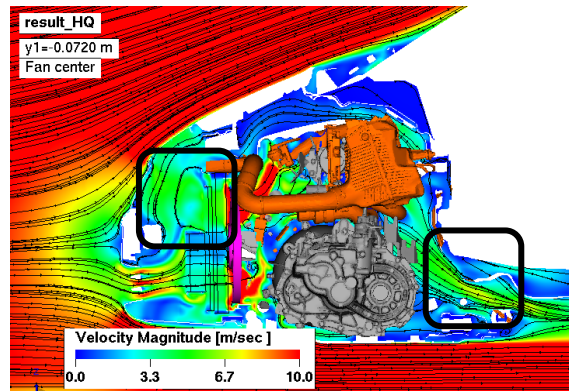


Figure 21. Velocity at fan center plane (Case 1)

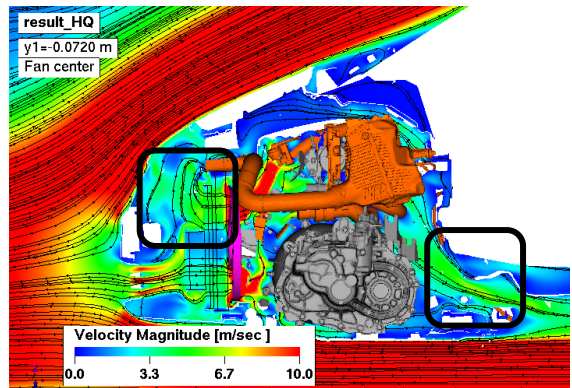


Figure 22. Velocity at fan center plane (Case 3)

Figure 23 and Figure 24 compare velocity distribution and streamlines at the top-right grille between cases 1 and 3. Lower velocity at the top grille and stronger recirculation in front of the heat exchangers were found in case 3 than case 1. These local small-scale flow structures are critical for optimization of the vehicle underhood design.

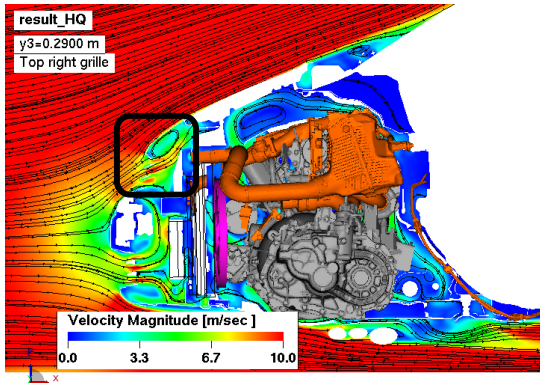


Figure 23. Velocity at fan center plane (Case 1)

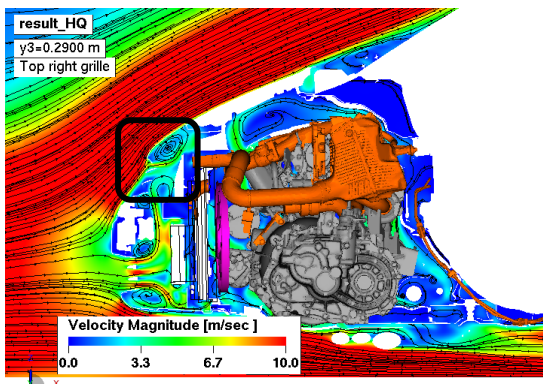


Figure 24. Velocity at fan center plane (Case 3)

Figure 25 and Figure 26 compare temperature distributions and streamlines at horizontal fan center plane between cases 1 and 3. Slightly higher air temperature around engine is observed in case 1 due to the better cooling performance.

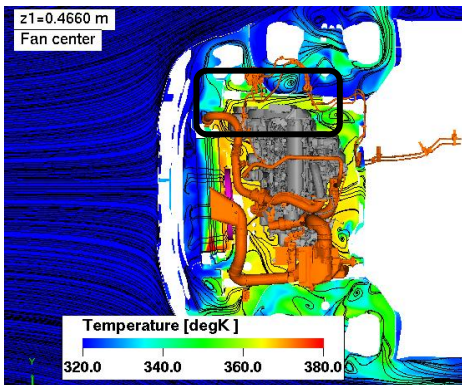


Figure 25. Temperature at the top grille (Case 1)

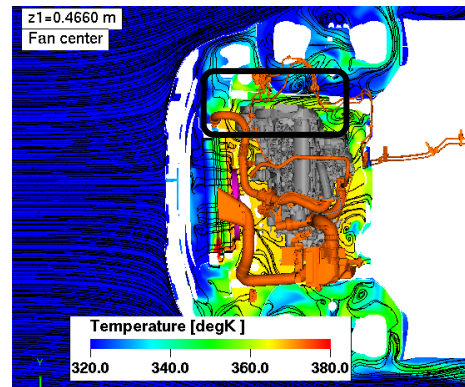


Figure 26. Velocity at the top grille (Case 3)

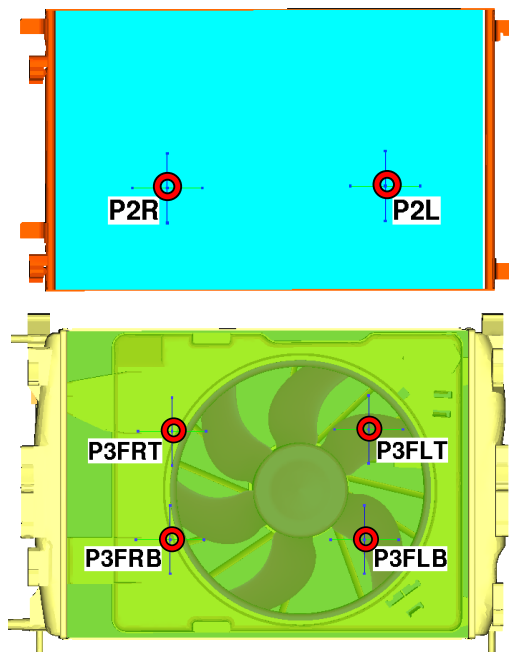


Figure 27. Locations and descriptions of the thermocouples before and after the condenser (front view)

The temperature averages were measured at the monitoring locations shown in Figure 27. The averaged fluid temperatures at these monitoring locations before and after condenser are summarized in Table 2. The difference of the probe temperature is within 1°C between cases 1 and 2. There is up to 3°C difference for top probes after condenser between cases 2 and 3. These small differences are caused by different air flow distribution within the underhood area.

Table 3 summarizes the averaged local heat transfer coefficients (HTCs) for several critical parts: engine, transmission and exhaust pipe. The local heat transfer coefficients are influenced by local air flow velocity. The averaged HTC for engine is slightly smaller in case 3 due to the lower air mass flow from the front grilles. Lower velocity was

identified around rear exhaust pipe which leads to lower averaged HTC's in case 2. Similarly, lower HTC's were found in case 3 and higher HTC's in case 2 for transmissions. These differences are within 20% which can result in significant difference in fluxes prediction. In addition, these differences do not change linearly with nozzle sizes. This result points to potential nozzle size related issues where the measurement configuration can significantly influence the measured part cooling rate. Such measurement related dependency can result in very misleading measured values.

TEMP [°C]	P2L	P2R	P3FLT	P3FRT	P3FLB	P3FRB
CASE 1	71.6	55.5	62.2	84.7	72.9	70.3
CASE 2	71.4	55.5	61.7	83.7	72.9	70.4
CASE 3	71.3	55.2	63.9	86.7	72.8	70.2

Table 2. Comparison between experimental and averaged predicted fluid temperature

Averaged Local HTC's [Watt/(m ² ·°K)]	CASE 1	CASE 2	CASE 3
Engine	2.7	2.7	2.6
Transmission	5.2	5.6	4.7
Exhaust Pipe	8.8	7.2	8.7

Table 3. Heat transfer coefficients comparison

The mass flow rates through the top and bottom grilles are summarized in Table 4. The mass flow rates through the grilles in case 1 is less than in the thermal wind tunnel simulation. Lower thermal performance of the cooling air expected for all three cases in digital wind tunnel. The mass flow rate through the top grille in case 2 is slightly lower than in case 1. But the mass flow rate through the top grille is much lower in case 3. Because of the thinner high speed layer above the vehicle hood and larger changes of air velocity direction in case 3, less air flow is passing through the top grille.

Mass Flow Rate [kg/s]	Case 1 (full size)	Case 2 (3/4 size)	Case 3 (half size)	Thermal Wind Tunnel
Top Grille	0.244	0.239	0.152	0.268
Bottom Grille	0.553	0.555	0.580	0.624

Table 4. Mass flow rates comparison between three nozzle sizes and the thermal wind tunnel

Table 5 summarizes the mass flow rates of the three heat exchangers respectively. Although different mass flow rates through the grille, the difference of the mass flow rates through the heat exchangers is very small. There is almost no change between the cases 1 and 2. In case 3, the air mass flow rate of the condenser is about 1% less than for the case 1, and air mass flow through the radiator is 2% less.

Mass Flow Rate [kg/s]	CAC	CON	RAD
Case 1	0.226	0.500	0.573
Case 2	0.227	0.500	0.571
Case 3	0.228	0.496	0.561

Table 5. Mass flow rate of heat exchangers

HEAT REJECTION [kW]	CAC	CON	RAD
CASE 1	5.08	5.84	15.73
CASE 2	5.08	5.46	15.48
CASE 3	5.08	5.49	15.29

Table 6. Heat rejection comparison

Table 6 summarizes the heat rejections of the three heat exchangers respectively. The heat rejection not only depends on the averaged airflow velocity and temperature but also on the uniformity of the velocity distribution of air right in front the heat exchangers. The heat rejection of the radiator reduces by 1.6% for case 2 and by 2.8% for case 3 respectively.

CONCLUSIONS

Presented were simulations of the cooling airflow and external aerodynamics for Renault Scenic II in the digital wind tunnel with three nozzle sizes. The simulation methodology based on the coupling between the flow solver and the system tool can be used to study the airflow effects on the thermal performance. Comparison between the three simulation results has demonstrated that different nozzle sizes do impact the air flow in front of the vehicle and the resulting thermal performance of the cooling airflow. Even though almost identical heat rejections for the cooling package were predicted, indicating almost identical flow conditions, significant differences in the order of 20% were observed for transmission and exhaust cooling rates.

ACKNOWLEDGMENTS

The authors thank Renault for providing the test results and practical background on thermal wind tunnel operation.

REFERENCES

- [1] K. Srinivasan, Z.J. Wang, W. Yuan, R. Sun, "Vehicle thermal management simulation using a rapid omni-tree based adaptive Cartesian mesh generation methodology," HT-FED 2004-56748, 2004 ASME Heat Transfer/Fluids Engineering Summer Conference, July 11-15, Charlotte, North Carolina, USA.
- [2] B. Uhl, F. Brotz, J. Fauser, U. Krueger, "Development of engine cooling systems by coupling CFD simulation and heat exchanger analysis programs," SAE 2001-01-1695.
- [3] G. Seider, F. Bet, T. Heid, U. Hess, T. Klein, and J. Sauer, "A numerical simulation strategy for complex automotive cooling systems," SAE 2001-01-1722.
- [4] H. Knaus, C. Ottosson, F. Brotz, W. Kuehnel, "Cooling module performance investigation by means of underhood simulation," SAE 2005-01-2013.
- [5] T.P. Nobel, S.K. Jain, "A multidimensional approach to truck underhood thermal management," SAE 2001-02-2785.
- [6] C.L.R.Siqueira, P. Vatauvuk, M. Jokuszies, M.R. Lima, "Numerical simulation of a truck underhood flow," SAE 2002-01-3453.
- [7] E.A. Costa, "CFD approach on underhood thermal management of passenger cars and trucks," SAE 2003-01-3577.
- [8] F. Fortunato, F. Damiano, L. Di Matteo, P. Oliva, "Underhood cooling simulation for development of new vehicles," SAE 2005-01-2046.
- [9] A. Alajbegovic, R. Sengupta, W. Jansen: "Cooling Airflow Simulation for Passenger Cars using Detailed Underhood Geometry," SAE 2006-01-3478, SAE Conference, Chicago, October 2006
- [10] B. Xu, A. Konstantinov, J. Amodeo, W. Jansen, A. Alajbegovic, "Simulation of Cooling Airflow under Different Driving Conditions," SAE 2007-01-0766, SAE World Congress, Detroit, April 2007
- [11] S. Brémont, G. Servera, E. Fares, J. Abanto, A. Alajbegovic: "Experimental Investigation and Numerical Validation of Cooling Airflows of a Realistic Vehicle," 6th FKFS Conference, Stuttgart, Germany, October 2007
- [12] Bhatnager, P., Gross, E. and Krook, M., "A Model for Collision Processes in Gases. I. Small Amplitude processes in Charged and Neutral One-component System", Phys. Rev., Vol. 94, pp. 511-525, 1954
- [13] S. Chen and G. D. Doolen, "Lattice Boltzmann method for fluid flows", *Annual Review of Fluid Mechanics*, 30:329-364, 1998.
- [14] U. Frisch, B. Hasslacher, and Y. Pomeau, "Lattice gas automata for the Navier-Stokes equation," *Physical Review Letters*, 56:1505-1508, 1986.
- [15] S. Succi, *The Lattice Boltzmann Equation for Fluid Dynamics and Beyond*, Series Numerical Mathematics and Scientific Computation, Clarendon Press, Oxford, 2001.
- [16] D. d'Humieres, P. Lallemand and Y. H. Quian, "Lattice BGK models for Navier-Stokes equations," *Europhysics Letters*, 17(6):479-484, 1992.
- [17] V. Yakhot, and S.A. Orszag, "Renormalization Group Analysis of Turbulence. I. Basic Theory" *J. Sci. Comput.*, 1(2), 3-51, 1986.
- [18] V. Yakhot, V., S.A. Orszag, S. Thangam, T. Gatski, and C. Speziale, "Development of turbulence models for shear flows by a double expansion technique," *Phys. Fluids A*, 4 (7), 1510-1520, 1992.
- [19] H. Chen, S.A. Orszag, I. Staroselsky, and S. Succi, "Expanded Analogy between Boltzmann Kinetic Theory of Fluid and Turbulence", *J. Fluid Mech.*, 519: 307-314, 2004.
- [20] H. Chen, "H-theorem and generalized semi-detailed balance conditions for lattice gas systems," *J. Stat. Phys.* 81:347-359, 1995.
- [21] H. Chen and C. Teixeira, "H-Theorem and origins of instability in thermal lattice Boltzmann models," *Comp. Phys. Communication*, 129:21-31, 2000.
- [22] H. Chen and R. Zhang, "Lattice Boltzmann method for simulations of liquid-vapor thermal flows," *Phys. Rev. E*67(6): Art. no. 066711 Part 2, 2003.
- [23] C. M. Teixeira, "Incorporating turbulence models into the lattice-Boltzmann method," *Int. J. Modern Physics C*, 9(8):1159-1175, 1998.
- [24] PowerFLOW User's Guide, Release 4.1, Exa Corporation, Boston, Massachusetts, 2007